# Size-Dependent Correlations between Strain and Phonon Frequency in Individual ZnO Nanowires

Xue-Wen Fu, Zhi-Min Liao,* Ren Liu, Jun Xu, and Dapeng Yu*

State Key Laboratory for Mesoscopic Physics, Department of Physics, Peking University, Beijing 100871, People's Republic of China

**ABSTRACT** The effect of uniaxial tensile strain on individual ZnO nanowires with diameters ranging from 500 nm to 2.7 $\mu$m and the effect of pure bending strain on ZnO microwires are systematically investigated by Raman spectroscopy. It is found for the first time that the tensile and compressive strains result in a linear downshift and upshift of the phonon frequencies of the $E_{2L}$, $E_{2H}$, $E_{1TO}$, and second-order modes compared with the strain-free state, respectively, while the $A_{1TO}$ mode is not influenced by the strain. Furthermore, the strain modulation on phonons depends strongly on the nanowire diameter. The $E_{2H}$ phonon deformation potential is ~3 cm$^{-1}$/% for the 500 nm nanowire, while 1% tensile strain results only in ~1 cm$^{-1}$ downward frequency shift for the 2.7 $\mu$m ZnO wire. The results provide a versatile "local-self-calibration" and nondestructive method to measure and monitor the local strains in ZnO micro/nanostructures.
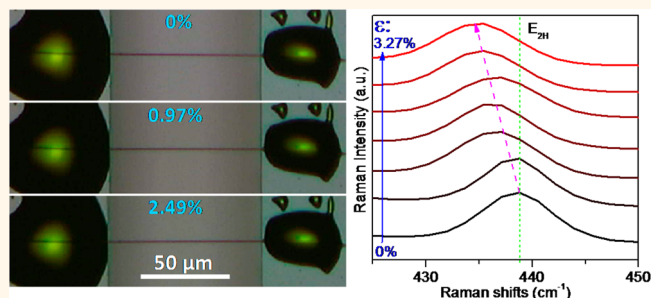
**KEYWORDS:** ZnO nanowires · uniaxial tensile strain · Raman spectrum · pure bending strain · size effect

Continuous modulation of the optical, transport, and carrier—phonon interaction properties of semiconductors is imperative for improving the performance of optoelectronic devices.[1−3] Elastic strain engineering has been proposed as a low-cost and continuously variable manner for controlling materials properties. Recently, strain engineering of semiconductor nanostructures has attracted great interest due to the much higher elastic limit compared to bulk materials.[4−9] It has been demonstrated that strain can effectively tune the properties of semiconductor nanostructures, such as enhancement of carrier mobility in Si nanotransistors by elastic local strain,[10] tension strain induced giant and abnormal piezoresistance in Si[11,12] and Ge[13] nanowires (NWs), and linear red-shift of the band gap in GaAs[14] and CdS[15] NWs. Particularly, elastic strain engineered ZnO NWs have significant advantages due to the coupling of piezoelectric and semiconducting properties. For example, strained ZnO NWs have great potential applications for the nanogenerators,[16] piezophototronic devices,[3,17] and strain gauges.[18] Strain can also modulate the band gap of ZnO NWs.[19−23] It is demonstrated that the tensile strain modulation on the band gap of ZnO NWs is strongly size-dependent.[24] Therefore, strain engineering is an effective route to tune the electronic band structures of ZnO NWs.[25] However, the strain effect on phonon modes of individual ZnO nano/microwires is still elusive.

In this work, we report the modulation of optical phonons in individual ZnO nano/microwires *via* uniaxial tensile strain and bending strain employing Raman spectroscopy. It is novel to find that the frequencies of the $E_{2H}$, $E_{1TO}$, and second-order phonons of ZnO NWs linearly red-shift with the increasing tensile strain, while the $A_{1TO}$ phonon has no response to strain. The tensile strain modulation on phonon frequency is also strongly dependent on the diameter of the ZnO NWs. Furthermore, our Raman mapping results of a pure bent ZnO microwire demonstrate that the local tensile and compressive strains result in a linear red-shift and blue-shift of the $E_{2H}$, $E_{1TO}$, second-order, and $E_{2L}$ phonon frequencies, respectively, and the $A_{1TO}$ phonon is rather robust and is not affected by the strain. On the
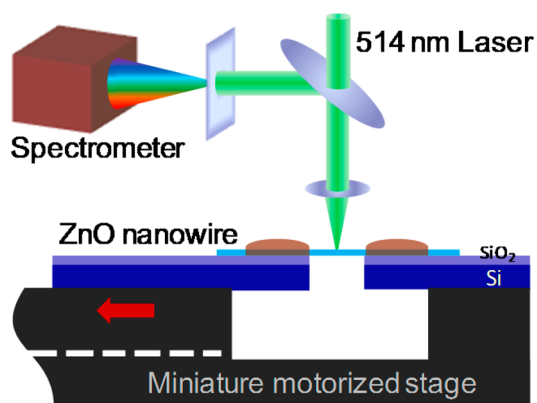
Figure 1. Schematic illustration of the Raman measurements. The Raman spectra can be measured for a suspended ZnO NW with different tensile strains, which are produced by a miniature linear stage with single-axis motorized movement.

basis of these novel results, local strains can be measured through analyzing the relative position of the $E_{2H}$ Raman peak with respect to the $A_{1TO}$ peak. This provides a versatile "local-self-calibration" and nondestructive method to monitor the local strains in semiconductor micro/nanostructures.

## RESULTS AND DISCUSSION

**Raman Spectra of Strain-Free and Suspended ZnO Nanowires.** The ZnO NWs were synthesized by the chemical vapor phase deposition (CVD) technique.[26,27] The high-quality ZnO NWs grow along the [0001] direction, with diameters ranging from 300 nm to 3.5 $\mu$m and lengths of hundreds of micrometers (Supplementary Figure S1). Figure 1 illustrates the Raman spectrum measurement for individual ZnO NWs. A ZnO nanowire was suspended on the miniature motorized stage with its c-axis along the tension direction. To avoid slippage of the NW on the substrate, both ends of the NW were firmly fixed on the SiO$_2$/Si pads by a kind of glue. The initial gap width $L_0$ and elongation $\Delta L$ of the NW under loading were determined in situ by optical imaging, and the uniaxial tensile strain in the individual NWs is $\varepsilon_c = \Delta L/L_0$. All the Raman spectra were recorded with the polarization of the incident laser perpendicular to the c-axis of the ZnO NWs. Prior to stretching the ZnO NW, Raman spectra were collected at three different positions along the NW, as shown in Figure 2a. The Raman spectra exhibit identical characteristics at the three different positions, as shown in Figure 2b, indicating that the ZnO NW is highly homogeneous.

The wurtzite structure ZnO belongs to the $C_{6v}^4$ (P6$_3$mc) space group. The zone-center optical phonon modes can be classified by the following irreducible representations: $\Gamma_{opt} = A_1 + E_1 + 2E_2 + 2B_1$. The $B_1$ branches are inactive modes. The $A_1$ branch originates from the ion vibrations along the c-axis (Figure 2c), and the $E_1$ branch is related to the ion vibrations perpendicular to the c-axis. The $A_1$ and $E_1$ branches are polar modes, and they split into longitudinal-optical (LO) and
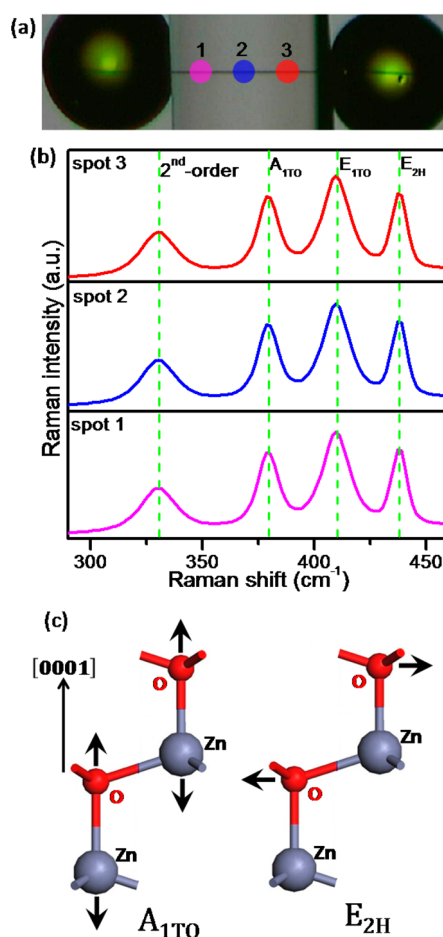


Figure 2. Raman spectra of a strain-free ZnO nanowire. (a) Optical image of a strain-free suspended ZnO NW with a diameter of 950 nm. (b) Raman spectra of the strain-free ZnO NW at three different spots, as indicated in (a). The Raman spectrum exhibits four intensive Raman peaks at 437.8 cm$^{-1}$ ($E_{2H}$), 409.6 cm$^{-1}$ ($E_{1TO}$), 378.6 cm$^{-1}$ ($A_{1TO}$), and 332.1 cm$^{-1}$ (second-order) in the measurement range. (c) Schematic diagram of atomic vibrations for the $A_{1TO}$ and $E_{2H}$ phonon modes in wurtzite ZnO.

transverse-optical (TO) components with different frequencies. The two $E_2$ branches are nonpolar phonons. The high-frequency $E_2$ mode ($E_{2H}$) is associated with O motion (as illustrated in Figure 2c), and the low-frequency $E_2$ mode ($E_{2L}$) is mainly associated with Zn motion.[28−31] The multiple zone boundary phonon scattering process gives rise to a second-order Raman peak. As shown in Figure 2b, the Raman spectrum of the strain-free NW exhibits four intensive peaks centered at 437.8, 409.6, 378.6, and 332.1 cm$^{-1}$, which are assigned to the $E_{2H}$, $E_{1TO}$, $A_{1TO}$, and the second-order phonon modes, respectively.[28,29]

**Raman Spectra of ZnO Nanowires under Tensile Strains.** To explore the influence of the uniaxial tensile strain on the phonon modes of ZnO NWs, we measured a series of Raman spectra of individual ZnO NWs with different diameters under different loadings. For the Raman measurements of the nanowire under uniaxial strain, the laser spot focuses on the center of the suspended
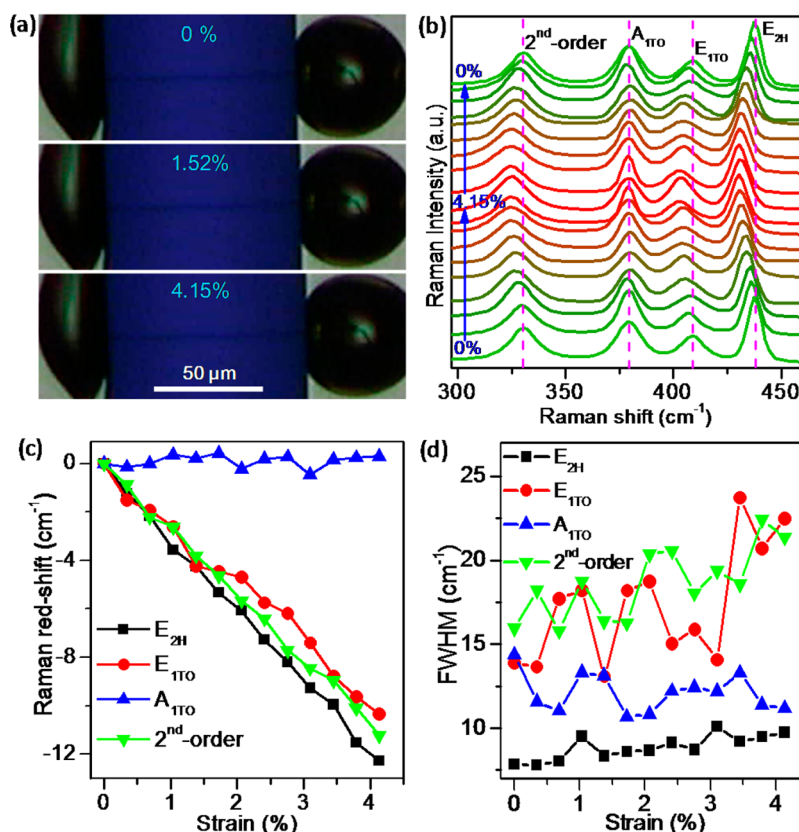
**Figure 3. Raman spectra of a ZnO nanowire under different tensile strains.** (a) Optical images of the ZnO NW with a diameter of 500 nm with different tensile strains. (b) Raman spectrum evolution with uniaxial tensile strains from 0% to 4.15% and then back to 0%. The pink dashed lines indicate the Raman peak positions at the strain-free state. (c) Phonon frequency shifts of $E_{2H}$, $E_{1TO}$, $A_{1TO}$, and second-order modes as a function of tensile strain value. (d) Variation of full width at half-maximum of these four Raman peaks *versus* the tensile strain.

nanowire. After each strain loading, the laser spot was adjusted to keep focusing on the center of the nanowire under a confocal micro-Raman microscope. Besides that, to further confirm the reliability of the experiment data, we also measured the Raman spectra from three different positions along the suspended nanowire under a certain strain loading, and it is found that the Raman spectra exhibit identical characteristics at the three different positions, as presented in Figure S2.

Figure 3 shows the typical results of a ZnO NW with a diameter of 500 nm. Figure 3a shows the optical images of the ZnO NW under different tensile loadings. The ZnO NW was stretched step by step with a tensile strain of up to 4.15%. Figure 3b presents the evolution of the Raman spectra with increasing uniaxial tensile strains from 0% to 4.15% and then back to 0%. It is interesting to note that the $E_{2H}$, $E_{1TO}$, and second-order phonon frequencies first downward shift with increasing tensile strain up to 4.15% and then shift back to the original positions upon releasing the tensile strain to 0%. The $E_{2H}$, $E_{1TO}$, and second-order peaks downward shift by 12.3, 10.3, and 11.2 cm$^{-1}$ at a tensile strain of 4.15%, respectively. Nevertheless, it is surprising to find that the $A_{1TO}$ peak has no obvious change and exhibits a constant peak position within the experimental accuracy while varying the tensile strain. The fact that

the $A_{1TO}$ phonon mode is not sensitive to the tensile strain is quite different from the previous results observed through a hydrostatic pressure test on bulk ZnO crystal, where it was demonstrated that all the phonon modes in bulk ZnO are sensitive to the hydrostatic pressure.[29,32] This discrepancy is probably due to the different strain loading methods. The hydrostatic pressure exerts isotropic strain on the ZnO crystal and results in isotropic compression of the lattice, while the uniaxial tensile strain in our experiment results in elongation of the lattice along the c-axis and shrinkage of the a–b plane to maintain the Poisson ratio.

Figure 3c shows the $E_{2H}$, $E_{1T}$, $A_{1TO}$, and second-order phonon frequency variations as a function of tensile strain value. Except for $A_{1TO}$, the red-shifts of the $E_{2H}$, $E_{1T}$, and second-order phonon frequencies linearly increase with increasing uniaxial tensile strain. The linear relationship between the phonon frequency red-shift $\Delta\omega$ and the uniaxial tensile strain $\varepsilon_c$ is given by $\Delta\omega = \gamma\varepsilon_c$, where $\gamma$ is the phonon deformation potential coefficient. From linear fittings in Figure 3c, we can obtain $\gamma$ values of $-2.99$, $-2.47$, and $-2.69$ cm$^{-1}$/% for the strain-sensitive $E_{2H}$, $E_{1TO}$, and second-order modes, respectively. Figure 3d shows the variations of full width at half-maximum (FWHM) of the Raman peaks as a function of tensile strain. The Raman peaks are

not significantly broadened with increasing tensile strain. The Raman peak broadening is mainly due to the relaxation of the wave-vector selection rule.[33] Under strain situations, the phonon scattering will not be limited in only the Brillouin center and the phonon dispersion near the zone center must also be considered, which results in the slight broadening of the Raman peak.

For the wurtzite ZnO crystal, the zone center phonons are related to the atomic vibrations. The tensile strain along the $c$-axis will weaken the bond interaction and lower the atomic vibration frequency from the $E_{2H}$, $E_{1TO}$, and second-order modes and thus lead to the red-shift of the Raman peak. The $A_{1TO}$ phonon mode in the ZnO crystal originates from the vibration of atoms along the $c$-axis, as schematically shown in Figure 2c. The frequency behaviors of the $A_{1TO}$ phonon in ZnO nanowires under uniaxial $c$-axis strain can be understood by analyzing the frequency variation of a harmonic oscillator in a one-dimensional atomic chain. Assuming that the oscillator has a stiffness factor of $k$ and a mass of $m$ under a constant small stretching force $F_0$ that causes a displacement $x_0$ away from the equilibrium position with $F_0 = -kx_0$, then we have the dynamic equation $m(d^2x/dt^2) = -kx + F_0$, where $x$ is the displacement away from the equilibrium position. The equation can be reformed as $[d^2(x - x_0)]/dt^2 + (k/m)(x - x_0) = 0$, which still has the same vibration frequency $\omega_0 = (k/m)^{1/2}$. The extra force or deformation along the vibration direction cannot change the vibration frequency of the harmonic oscillator. For the $A_{1TO}$ phonon mode in the ZnO nanowire under uniaxial $c$-axis strain, it is very similar to the oscillator under a stretching force and its frequency should not change either, as observed in our experimental results.

**Size-Dependent Phonon Deformation Potential.** The ZnO nanowire diameter dependence of the tensile strain modulation of the phonons was further studied. As detailed in the Supplementary Figures S3−S6, similar Raman spectra evolution and the linear frequency red-shifts of the tensile strain sensitive phonon modes were also observed in the ZnO NWs with diameters ranging from 500 nm to 2.7 $\mu$m. We summarize the data of tensile strain induced red-shift of the $E_{2H}$ mode ($E_{1TO}$ and second-order modes have the same tendency) of the ZnO NWs with different diameters in Figure 4a. From the slopes of the $\Delta\omega$ vs $\varepsilon_c$ curves, it is shown distinctly that the phonon deformation potential coefficient is strongly size-dependent. The absolute value of the $E_{2H}$ phonon deformation potential increases with decreasing NW diameter, as shown in Figure 4b. For the 500 nm nanowire, the phonon deformation potential is ∼3 cm$^{-1}$/$\varepsilon$%, while the $E_{2H}$ phonon frequency shifts about 1 cm$^{-1}$ by 1% strain for the largest ZnO wire (2.7 $\mu$m) in our experiment. The reported phonon deformation potential is 2.94 cm$^{-1}$/GPa for the $E_{2H}$ phonon under uniaxial pressure.[34] To compare with our results, the applied load GPa should
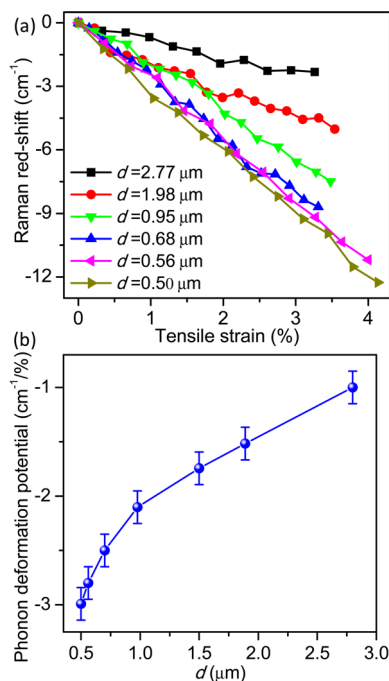


Figure 4. Size-dependence of strain-modulated phonon frequency. (a) Tensile strain $vs$ phonon frequency red-shift of the $E_{2H}$ mode for ZnO NWs with different diameters. (b) Phonon deformation potential of the $E_{2H}$ mode as a function of ZnO NW diameter.

be converted to strain value (%). Under the uniaxial $c$-axis pressure, due to the Poisson effect $\varepsilon_{xx} = \varepsilon_{yy} = -v\varepsilon_{zz}$, where $v$ is the Poisson's ratio, the total strain $\varepsilon = (1 - 2v)\varepsilon_{zz}$. Therefore, the phonon deformation potential is formed as $\partial(\Delta\omega)/(\partial\varepsilon) = (1 - 2v)E_b[\partial(\Delta\omega)/\partial\sigma_{zz}]$, where $E_b \approx 140$ GPa is the Young's modulus along the $c$-axis,[35] and the Poisson's ratio of ZnO is 0.353.[36] Therefore, we can estimate that 1% strain should produce a shift of about 1.2 cm$^{-1}$ for the $E_{2\text{-high}}$ phonon for bulk ZnO crystal reported by Callsen et al.,[34] which is generally consistent with the result (∼1 cm$^{-1}$/$\varepsilon$%) of the large wires in our work. This indicates that the phonon deformation potential value would approach the bulk limit with increasing NW diameter.

The size dependence of the $E_{2H}$ phonon deformation potential may originate from the surface effect due to the large surface-to-volume ratio of the ZnO NWs. It is known that the surface reconstruction will cause shrinkage of the Zn−O bond,[37] and recently it has been experimentally observed using aberration-corrected transmission electron microscopy (TEM).[38] For the same strain value, the surface will endure larger stress than that of bulk ZnO crystal, resulting in the increase of the Raman peak shift. The measured Raman spectrum can be considered from both the surface region and the core region. With decreasing the nanowire diameter, the surface-to-volume ratio will increase and the surface shrinking effect will be more notable. Therefore, the phonon deformation potential increases with decreasing the nanowire diameter.
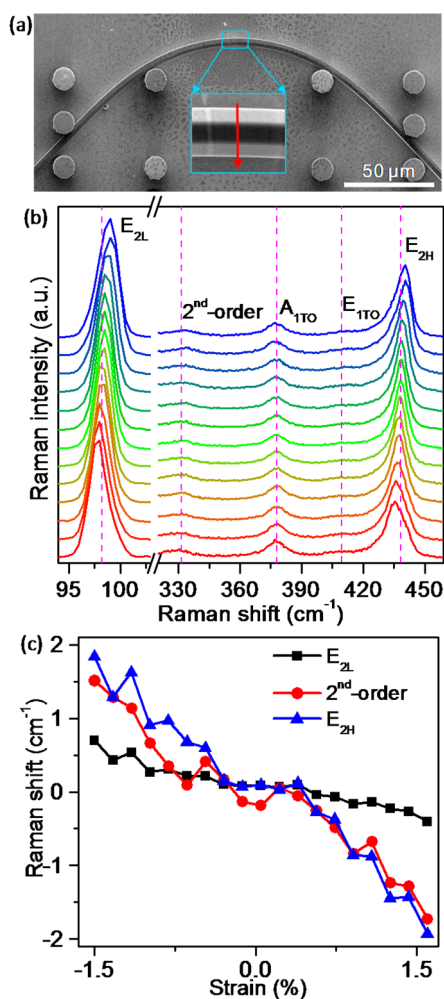
**Figure 5.** Raman spectra of a pure bent ZnO microwire. (a) SEM image of a four-point-bending ZnO MW with a diameter of 3.4 $\mu$m. (b) Raman spectra from bottom to top in the panel are acquired along the line scanning from tensile to compressive edges in the pure bending region. (c) Phonon frequency shifts of $E_{2L}$, $E_{2H}$, and second-order modes as a function of the bending stain. Plus means the tensile strain and minus means the compressive strain.

**Raman Spectra of a Pure Bent ZnO Microwire.** In order to correlate the Raman spectrum evolution with compressive strain, an individual ZnO microwire (MW) was manipulated by two glass tips under a microscope to form the standard four-point-bending configuration and acquire a pure bent region. As shown in Figure 5a, a ZnO MW with a diameter of 3.4 $\mu$m is stuck in the middle of the prefabricated four supporting pillars (SU8). The middle segment of the bent ZnO MW is in a pure bending state without shear strain. The $c$-axis strain from the inner side to the outer side across the ZnO wire diameter is given by $\varepsilon_c = \pm r/\rho$, where $\rho$ is the local curvature radius and $r$ is the distance away from the strain-neutral plane. The negative and positive values of $\varepsilon_c$ represent the compressive and tensile strains, respectively. We collected the Raman spectra step by step (300 nm in step length) from tensile to compressive edges along one pure bending

cross-section, as indicated by the red arrow in the inset in Figure 5a, and the corresponding Raman spectra are shown in Figure 5b in order from bottom to top. For this experimental setup, the wavenumber can be down to 80 cm$^{-1}$, and the $E_{2L}$ Raman peak centered at 98.4 cm$^{-1}$ at the strain-free region was observed. Similarly, except for the $A_{1TO}$ mode, all the other Raman peaks are sensitive to the strain. The phonon frequencies linearly downshift with increasing tensile strain from the neutral plane to the outer edge, while linearly upshift with increasing compressive strain from the neutral plane to the inner edge (see Figure 5c). By linear fitting of the data in Figure 5c, the phonon deformation potentials of $-0.27$, $-0.82$, and $-1.06$ cm$^{-1}$/% for the $E_{2L}$, second-order, and $E_{2H}$ modes are obtained, respectively. It is worth noting that the phonon deformation potential of the $E_{2H}$ mode obtained by the pure bending test is in good agreement with the uniaxial tensile result of the large wire. It is also close to the limiting case of bulk ZnO, again indicating the reliability of our uniaxial tensile results. Through monitoring the variation of the $E_{2H}$ mode, the most strain-sensitive phonon mode, the local strain in the ZnO nano/microwires can be probed.

Figure 6a,b show the Raman mappings of the $E_{2H}$ peak position and FWHM, respectively. The striking contrast of the color from tensile (position marked by plus) side to compressive (position marked by minus) side shows the variations of the $E_{2H}$ mode in the pure bending region. The $E_{2H}$ phonon frequency changes continuously from tensile to compressive edges, and both the tensile and compressive strains can cause Raman peak broadening. For comparison, the Raman mappings of the $A_{1TO}$ peak position and FWHM are shown in Figure 6c and d, respectively. There are no obvious color contrasts in both of them, suggesting that the $A_{1TO}$ phonon mode does not respond to the bending strain in the pure bent ZnO MW, which is also in agreement with the uniaxial tensile results.

**Discussion.** Confocal $\mu$-Raman microscopy has been used to study strained semiconductor nanostructures with high spatial resolution by analyzing the Raman peak broadening.[39] Raman peak broadening was observed in bent InP nanowires due to the inside compressive and outside tensile strains.[39] However, the method employing Raman peak broadening to probe the strain is limited to the bending strains, is highly influenced by the laser spot size and the nanowire diameter, and is necessary to measure the Raman spectrum of the nanowire at the strain-free state for reference. On the other hand, the Raman peaks may also vary with the size of the strain-free nanowire due to the surface atomic relaxation. Thus in the low-dimensional semiconductor micro/nanostructures, it is hard to identify the local strain from the shift of each Raman peak compared with that of the strain-free bulk material. Fortunately, our experimental results reveal that the $A_{1TO}$ phonon peak of ZnO NWs does not change under uniaxial or pure bent
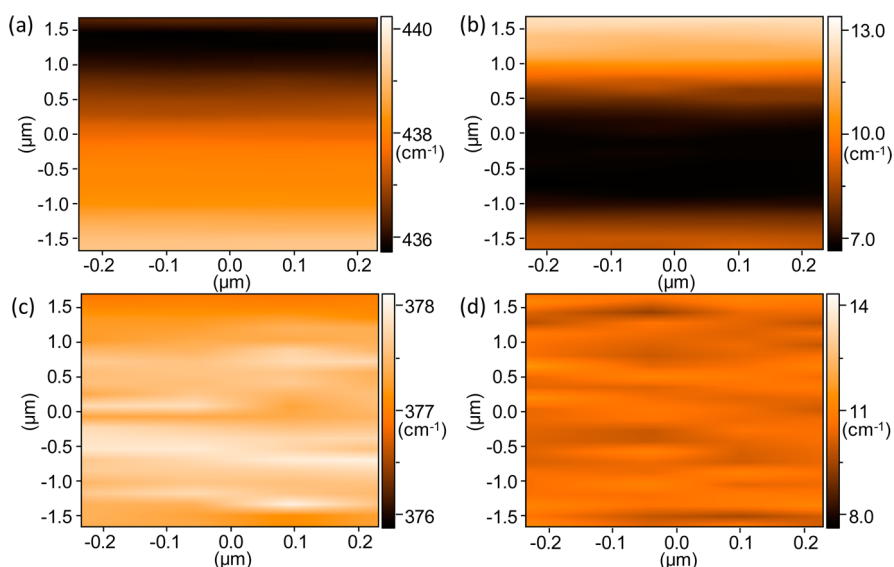
**Figure 6. Raman mappings of a pure bent ZnO microwire. (a, b) Raman mappings of the $E_{2H}$ peak position and FWHM in the pure bending region of the ZnO microwire with a diameter of 3.4 $\mu$m, respectively. (c, d) Raman mappings of the $A_{1TO}$ peak position and FWHM in the pure bending region, respectively.**

strain. We also summarized the $A_{1TO}$ phonon frequency of the strain-free ZnO NWs with different diameters (see Figure S7), which does not significantly change upon varying the nanowire size. Therefore, the local strain can be precisely determined by analyzing the phonon frequency difference between the strain-sensitive Raman peak (such as $E_{2H}$) and the $A_{1TO}$ peak and considering the size-dependent coefficient as presented in Figure 4b. This *in situ* "local-self-calibration" and nondestructive method should be versatile to accurately monitor the local strain in ZnO nanostructures.

## CONCLUSIONS

In summary, we found that the $E_{2H}$, $E_{1TO}$, and second-order phonon frequencies decrease with increasing uniaxial tensile strain in ZnO NWs, whereas the $A_{1TO}$ phonon mode does not respond to strain. Furthermore, the tensile strain modulation on phonons is strongly size-dependent. The phonon deformation potential of the $E_{2H}$ mode increases from 0.7 to 3 cm$^{-1}$/% as the nanowire diameter decreases from 2.7 $\mu$m to 500 nm. Raman mapping results on the pure bent ZnO MW demonstrate that the local tensile and compressive strains cause a linear downshift and upshift of the $E_{2L}$, $E_{2H}$, $E_{1TO}$, and second-order phonon frequencies, respectively, except for the nonresponsive $A_{1TO}$ mode. Our results pave the way for a new and versatile route for *in situ* "local-self-calibration" and nondestructive measurement of the local strains in ZnO micro/nanostructures and devices.

## MATERIALS AND METHODS

**ZnO Nanowire Synthesis.** The synthesis of ZnO NWs was carried out in a horizontal quartz tube furnace by simple chemical vapor deposition. The mixture of pure zinc oxide (99.9999%) and graphite powder (molar ratio of 1:1) was loaded in an alumina boat. Sapphire chips with (110) orientation were placed above the source powder as the collecting substrates. The boat was then placed at the center of the quartz tube and inserted into a rapid heating furnace. The system was purged using argon gas for more than 10 min. After this, the carrier gas argon was maintained at 200 sccm flow for nanowire growth. The furnace was heated to 1050 °C during 20 min, and then oxygen (3.0 sccm) was introduced as the reactive gas. After 30 min growth, the system was cooled to room temperature step by step and the substrate was covered by a layer of wax-like products.

**Suspended ZnO Nanowires.** After growth, the ZnO NWs were dispersed in alcohol, and then a drop of alcohol with nanowires was placed on a Si wafer. After the alcohol was volatilized, the ZnO NWs were left on the Si substrate. Two SiO$_2$/Si (300 nm/1 mm in thickness) wafers were fixed firmly on the two ends of a miniature motorized stage (MMT32-A). The individual ZnO NW of interest was then transferred to cross over the two wafers with the *c*-axis of the nanowire along the tension direction by two needle-shaped glass tips mounted on a micromanipulator with an optical microscope. We then put two microdrops of glue on the two ends of the nanowire to fix it on the SiO$_2$/Si wafers by a glass tip using the micromanipulator. For gluing, Gatan two-component epoxy was used, which is usually used for cross-section TEM sample preparation. To avoid wetting the nanowire surface, we waited more than 24 h to let the glue cure naturally at room temperature rather than heating for fast curing. The epoxy glue was then hardened enough to firmly fix the ends of the nanowire on the SiO$_2$/Si wafers. Because there is no glue on the suspended part of the nanowire, the Raman spectrum measurements are not affected by gluing the nanowire on the two Si wafers.

**Uniaxial Tensile Strain Loading.** The uniaxial tensile loading on the ZnO NWs was carried out by a sophisticated single-axis linear miniature motorized stage (MMT32-A). The movement of the stage was controlled by an electronic control unit with a step accuracy of 0.156 $\mu$m. The ZnO NWs bridging the two SiO$_2$/Si pads were stretched step by step precisely *via* controlling the stretched length. The uniaxial tensile strain can be relaxed through returning the stage back step by step.

**Raman Spectrum Measurement.** The Raman spectra of the ZnO NWs under tensile strains were measured by a confocal micro-Raman microscopy system (Renishaw Raman microprobe RM1000B). The Raman spectra were excited by a 514 nm Ar ion laser with a focused spot size of ~1 $\mu$m and a power of ~1.6 mW at room temperature. All the Raman spectra were fitted by a Lorentzian profile to determine the Raman peak position and the line width with an accuracy better than 1 cm$^{-1}$.

**Pure Bent ZnO Microwire.** To induce pure bending deformation in an individual ZnO microwire, arrays of SU8 (SU-8, 2015) photoresist pillars with a diameter of 6.0 $\mu$m and a height of 15.0 $\mu$m were fabricated on a Si substrate by photolithography and a developing process. The SU8 photoresist was spin coated on the Si substrate (500 rpm for 10 s and then 3000 rpm for 60 s) and then heated at 65 °C for 1 min and then at 95 °C for 3 min. The SU8 photoresist on the wafer was exposed under a UV lamp (12 s, 13 mW/cm$^2$) with a predesigned mask. Finally, the wafer was developed by developer solution. After that, a desirable ZnO microwire was transferred onto the prearranged substrate under an optical microscope by using two needle-shaped glass tips and manipulated to be stuck in the middle of four SU8 pillars to form the standard four-point-bending configuration. For this standard four-point-bending configuration, the bending part between the two inner SU8 pillars is expected to be in a pure bending strain state. Such pure bending deformation is elastic, because the curved microwire can resume its original straight state once the SU8 pillars are removed.

**Raman Mapping Measurement.** The Raman mapping measurements for a pure bent ZnO microwire were performed using an HR800 Jobin Yvon spectrometer equipped with an Olympus microscope and a cooled charge-coupled device. The spectra were excited by a 532 nm line of a solid-state laser, and the spot size of the focused laser is ~0.5 $\mu$m with power of about 1.0 mW. The polarization direction of the incident light was perpendicular to the c-axis of the microwire to obtain better signal-to-noise ratio, and the step size of the mapping test was 200 nm. Considering a ~0.5 $\mu$m laser spot size, there is some overlapping between the adjacent positions with a scanning step of 200 nm. However, the center position of the laser spot on the ZnO microwire still follows the motion of the sample stage. Although the real Raman mapping resolution may be worse than 200 nm, the changing tendency of the phonon frequency along the bending cross section from inside to outside of the 3.4 $\mu$m ZnO wire can be clearly revealed. The spectrometer slit was set to give a spectral resolution always better than 1 cm$^{-1}$. For this experimental setup, the lowest Raman wavenumber can reach 80 cm$^{-1}$, and the $E_{2L}$ peak can be detected. Through recording the Raman spectra point-by-point over the preselected pure bending region, spectral mapping can be obtained.

*Conflict of Interest:* The authors declare no competing financial interest.

*Supporting Information Available:* SEM and TEM images of the ZnO nanowires. Uniaxial tensile strain dependent Raman spectra of suspended ZnO wires with different diameters. This material is available free of charge via the Internet at http://pubs.acs.org.

## REFERENCES AND NOTES

1. Mcdonald, S. A.; Konstantatos, G.; Zhang, S.; Cyr, P. W.; Klem, E. J.; Levina, L.; Sargent, E. H. Solution-Processed PbS Quantum Dot Infrared Photodetectors and Photovoltaics. *Nat. Mater.* **2005**, *4*, 138–142.

2. Cazzanelli, M.; Bianco, F.; Borga, E.; Pucker, G.; Ghulinyan, M.; Degoli, E.; Luppi, E.; Véniard, V.; Ossicini, S.; Modotto, D. Second-Harmonic Generation in Silicon Waveguides Strained by Silicon Nitride. *Nat. Mater.* **2011**, *11*, 148–154.

3. Wang, Z. L. Piezopotential Gated Nanowire Devices: Piezotronics and Piezo-Phototronics. *Nano Today* **2010**, *5*, 540–552.

4. Roberts, M. M.; Klein, L. J.; Savage, D. E.; Slinker, K. A.; Friesen, M.; Celler, G.; Eriksson, M. A.; Lagally, M. G. Elastically Relaxed Free-Standing Strained-Silicon Nanomembranes. *Nat. Mater.* **2006**, *5*, 388–393.

5. Tombler, T. W.; Zhou, C.; Alexseyev, L.; Kong, J.; Dai, H.; Liu, L.; Jayanthi, C.; Tang, M.; Wu, S.-Y. Reversible Electromechanical Characteristics of Carbon Nanotubes under Local-Probe Manipulation. *Nature* **2000**, *405*, 769–772.

6. Wang, L.; Zheng, K.; Zhang, Z.; Han, X. Direct Atomic-Scale Imaging about the Mechanisms of Ultralarge Bent Straining in Si Nanowires. *Nano Lett.* **2011**, *11*, 2382–2385.

7. Hong, K.-H.; Kim, J.; Lee, S.-H.; Shin, J. K. Strain-Driven Electronic Band Structure Modulation of Si Nanowires. *Nano Lett.* **2008**, *8*, 1335–1340.

8. Stan, G.; Krylyuk, S.; Davydov, A.; Levin, I.; Cook, R. Ultimate Bending Strength of Si Nanowires. *Nano Lett.* **2012**, *12*, 2599–2604.

9. Ngo, L. T.; Almécija, D.; Sader, J. E.; Daly, B.; Petkov, N.; Holmes, J. D.; Erts, D.; Boland, J. J. Ultimate-Strength Germanium Nanowires. *Nano Lett.* **2006**, *6*, 2964–2968.

10. Leong, M.; Doris, B.; Kedzierski, J.; Rim, K.; Yang, M. Silicon Device Scaling to the Sub-10-nm Regime. *Science* **2004**, *306*, 2057–2060.

11. He, R.; Yang, P. Giant Piezoresistance Effect in Silicon Nanowires. *Nat. Nanotechnol.* **2006**, *1*, 42–46.

12. Milne, J.; Rowe, A.; Arscott, S.; Renner, C. Giant Piezoresistance Effects in Silicon Nanowires and Microwires. *Phys. Rev. Lett.* **2010**, *105*, 226802.

13. Greil, J.; Lugstein, A.; Zeiner, C.; Strasser, G.; Bertagnolli, E. Tuning the Electro-Optical Properties of Germanium Nanowires by Tensile Strain. *Nano Lett.* **2012**, *12*, 6230–6234.

14. Signorello, G.; Karg, S.; Björk, M. T.; Gotsmann, B.; Riel, H. Tuning the Light Emission from GaAs Nanowires over 290 meV with Uniaxial Strain. *Nano Lett.* **2012**, *13*, 917–924.

15. Fu, Q.; Zhang, Z. Y.; Kou, L.; Wu, P.; Han, X.; Zhu, X.; Gao, J.; Xu, J.; Zhao, Q.; Guo, W. Linear Strain-Gradient Effect on the Energy Bandgap in Bent CdS Nanowires. *Nano Res.* **2011**, *4*, 308–314.

16. Qin, Y.; Wang, X.; Wang, Z. L. Microfibre–Nanowire Hybrid Structure for Energy Scavenging. *Nature* **2008**, *451*, 809–813.

17. Yang, S.; Wang, L.; Tian, X.; Xu, Z.; Wang, W.; Bai, X.; Wang, E. The Piezotronic Effect of Zinc Oxide Nanowires Studied by in Situ TEM. *Adv. Mater.* **2012**, *24*, 4676–4682.

18. Wang, X.; Zhou, J.; Song, J.; Liu, J.; Xu, N.; Wang, Z. L. Piezoelectric Field Effect Transistor and Nanoforce Sensor Based on a Single ZnO Nanowire. *Nano Lett.* **2006**, *6*, 2768–2772.

19. Han, X.; Kou, L.; Lang, X.; Xia, J.; Wang, N.; Qin, R.; Lu, J.; Xu, J.; Liao, Z.; Zhang, X. Electronic and Mechanical Coupling in Bent ZnO Nanowires. *Adv. Mater.* **2009**, *21*, 4937–4941.

20. Dietrich, C.; Lange, M.; Klupfel, F.; Von Wenckstern, H.; Schmidt-Grund, R.; Grundmann, M. Strain Distribution in Bent ZnO Microwires. *Appl. Phys. Lett.* **2011**, *98*, 031105.

21. Xue, H.; Pan, N.; Li, M.; Wu, Y.; Wang, X.; Hou, J. Probing the Strain Effect on Near Band Edge Emission of a Curved ZnO Nanowire via Spatially Resolved Cathodoluminescence. *Nanotechnology* **2010**, *21*, 215701.

22. Han, X.; Kou, L.; Zhang, Z.; Zhang, Z.; Zhu, X.; Xu, J.; Liao, Z.; Guo, W.; Yu, D. Strain-Gradient Effect on Energy Bands in Bent ZnO Microwires. *Adv. Mater.* **2012**, *24*, 4707–4711.

23. Xu, S.; Guo, W.; Du, S.; Loy, M.; Wang, N. Piezotronic Effects on the Optical Properties of ZnO Nanowires. *Nano Lett.* **2012**, *12*, 5802–5807.

24. Wei, B.; Zheng, K.; Ji, Y.; Zhang, Y.; Zhang, Z.; Han, X. Size-Dependent Bandgap Modulation of ZnO Nanowires by Tensile Strain. *Nano Lett.* **2012**, *12*, 4595–4599.

25. Liao, Z.-M.; Wu, H.-C.; Fu, Q.; Fu, X.; Zhu, X.; Xu, J.; Shvets, I. V.; Zhang, Z.; Guo, W.; Leprince-Wang, Y. Strain Induced Exciton Fine-Structure Splitting and Shift in Bent ZnO Microwires. *Sci. Rep.* **2012**, *2*, 452.

26. Fu, X.-W.; Liao, Z.-M.; Xu, J.; Wu, X.-S.; Guo, W.; Yu, D.-P. Improvement of Ultraviolet Photoresponse of Bent ZnO Microwires by Coupling Piezoelectric and Surface Oxygen Adsorption/Desorption Effects. *Nanoscale* **2013**, *5*, 916–920.

27. Fu, X.-W.; Liao, Z.-M.; Zhou, Y.-B.; Wu, H.-C.; Bie, Y.-Q.; Xu, J.; Yu, D.-P. Graphene/ZnO Nanowire/Graphene Vertical Structure Based Fast-Response Ultraviolet Photodetector. *Appl. Phys. Lett.* **2012**, *100*, 223114.

28. Cuscó, R.; Alarcón-Lladó, E.; Ibanez, J.; Artus, L.; Jimenez, J.; Wang, B.; Callahan, M. J. Temperature Dependence of Raman Scattering in ZnO. *Phys. Rev. B* **2007**, *75*, 165202.

29. Decremps, F.; Pellicer-Porres, J.; Saitta, A. M.; Chervin, J.-C.; Polian, A. High-Pressure Raman Spectroscopy Study of Wurtzite ZnO. *Phys. Rev. B* **2002**, *65*, 092101.

30. Damen, T. C.; Porto, S.; Tell, B. Raman Effect in Zinc Oxide. *Phys. Rev.* **1966**, *142*, 570.

31. Alim, K. A.; Fonoberov, V. A.; Shamsa, M.; Balandin, A. A. Micro-Raman Investigation of Optical Phonons in ZnO Nanocrystals. *J. Appl. Phys.* **2005**, *97*, 124313.

32. Reparaz, J.; Muniz, L.; Wagner, M.; Goñi, A.; Alonso, M.; Hoffmann, A.; Meyer, B. Reduction of the Transverse Effective Charge of Optical Phonons in ZnO under Pressure. *Appl. Phys. Lett.* **2010**, *96*, 231906.

33. Wang, R.-P.; Zhou, G.-W.; Liu, Y.-L.; Pan, S.-H.; Zhang, H.-Z.; Yu, D.-P.; Zhang, Z. Raman Spectral Study of Silicon Nanowires: High-Order Scattering and Phonon Confinement Effects. *Phys. Rev. B* **2000**, *61*, 16827.

34. Callsen, G.; Reparaz, J.; Wagner, M.; Kirste, R.; Nenstiel, C.; Hoffmann, A.; Phillips, M. Phonon Deformation Potentials in Wurtzite GaN and ZnO Determined by Uniaxial Pressure Dependent Raman Measurements. *Appl. Phys. Lett.* **2011**, *98*, 061906.

35. Chen, C.; Shi, Y.; Zhang, Y.; Zhu, J.; Yan, Y. Size Dependence of Young's Modulus in ZnO Nanowires. *Phys. Rev. Lett.* **2006**, *96*, 075505.

36. Gercek, H. Poisson's Ratio Values for Rocks. *Intern. J. Rock Mech. Min. Sci.* **2007**, *44*, 1–13.

37. Kulkarni, A. J.; Zhou, M.; Ke, F. J. Orientation and Size Dependence of the Elastic Properties of Zinc Oxide Nanobelts. *Nanotechnology* **2005**, *16*, 2749–2756.

38. He, M. R.; Yu, R.; Zhu, J. Subangstrom Profile Imaging of Relaxed ZnO(10 10) Surfaces. *Nano Lett.* **2012**, *12*, 704–708.

39. Chen, J.; Conache, G.; Pistol, M.-E.; Gray, S. M.; Borgström, M. T.; Xu, H.; Xu, H.; Samuelson, L.; Håkanson, U. Probing Strain in Bent Semiconductor Nanowires with Raman Spectroscopy. *Nano Lett.* **2010**, *10*, 1280–1286.